Smart Structures and Systems, Vol. 7, No. 3 (2011) 199-211
DOI: http://dx.doi.org/10.12989/sss.2011.7.3.199

Design rules for creating sensing and self-actuating microcapsules

German V. Kolmakov, Victor V. Yashin and Anna C. Balazs*

Chemical Engineering Department, University of Pittsburgh, Pittsburgh, PA 15261, USA

(Received March 15, 2010, Accepted October 29, 2010)

Abstract. Using computational modeling, we design a pair of biomimetic microcapsules that exploit chemical mechanisms to communicate and alter their local environment. As a result, these synthetic objects can undergo autonomous, directed motion. In the simulations, signaling microcapsules release "agonist" particles, while target microcapsules release "antagonist" particles and the permeabilities of both capsule types depend on the local particle concentration in the surrounding solution. Additionally, the released nanoscopic particles can bind to the underlying substrate and thereby create adhesion gradients that propel the microcapsules to move. Hydrodynamic interactions and the feedback mechanism provided by the dissolved particles are both necessary to achieve the cooperative behavior exhibited by these microcapsules. Our model provides a platform for integrating both the spatial and temporal behavior of assemblies of "artificial cells", and allows us to design a rich variety of structures capable of exhibiting complex dynamics. Due to the cell-like attributes of polymeric microcapsules and polymersomes, material systems are available for realizing our predictions.

Keywords: computer modeling; microcapsules; artificial cells; self-propelled particles; soft active materials.

1. Introduction

Biological cells have evolved complex mechanisms that allow them to not only sense chemical gradients on a surface, but also to move in response to these gradients, i.e., undergo haptotaxis. Haptotactic migration is vital to a number of biological functions, including the recruitment of leukocytes to sites of infection or tissue injury. The elegance and efficiency of this stimuli-responsive motion has motivated scientists to design microscopic, synthetic objects that could mimic such cellular activity (Bhattacharya *et al*. 2009, Hong *et al.* 2010, Solon *et al.* 2006, Usta *et al.* 2008). This is a challenging task because the "machinery" necessary for both sensing and self-actuation must be integrated into the synthetic objects and thus, one must rely on fundamental physical and chemical phenomena to power this intrinsically biological behavior. In effect, one must introduce a hierarchy of interlocking processes so that these objects can recognize chemical changes in the environment and then spontaneously react to these changes in a dynamic and coherent manner.

Using computational modeling, we attempt to address this challenge by designing a pair of three-dimensional, interacting microcapsules that create their own chemical gradients on an underlying surface and in response to these gradients, undergo self-sustained motion. Through these studies, we

*Corresponding Author, Ph.D., E-mail: balazs@pitt.edu

formulate guidelines for fabricating a microscopic system that exhibits an autonomous, motion-based reaction to an environmental change. Furthermore, we uncover a range of collective behavior that emerges from the interactions between the microcapsules. Notably, there have been few studies to examine how cooperative interactions between microcapsules (Bhattacharya *et al*. 2009, Usta *et al.* 2008) or liquid droplets (Nakata *et al.* 2000, Toyota *et al.* 2009) can lead to self-propelled movement. An important motivation for focusing on microcapsules and droplets is that these objects can serve as micro-carriers or even micro-reactors (Sukhorukov *et al.* 2005). Self-propelled micro-carriers that transport payloads in a controllable manner would be valuable for a variety of microfluidic applications (Ebbens and Howse 2010, Weibel *et al.* 2005).

The specific micro-carriers that we consider in formulating our design rules are polymeric microcapsules synthesized via the layer-by-layer (LbL) approach (Peyratout and Dahne 2004, Stadler *et al.* 2009, Tiourina *et al.* 2002) or "polymersomes" (Bellomo *et al.* 2004, Discher *et al.* 1999, Hammer *et al*. 2008). Due to their distinctive features, such objects could be tailored to exhibit a range of biomimetic functionality (Stadler *et al.* 2009). In particular, the shells of these micro-carriers are sufficiently robust to act as a protective barrier, and adequately permeable for the controlled exchange of reagents with an external solution (Jones 2004). Furthermore, the permselectivity of the shells can be readily tuned (Bellomo *et al.* 2004, Hammer *et al*. 2008, Ma *et al.* 2006, Shchukin *et al.* 2006, Sukhorukov *et al.* 2001). Moreover, by functionalizing the shell's outer surface, these micro-carriers can bind to an underlying substrate (Hammer *et al*. 2008). The LbL microcapsules can encapsulate nanoparticles and can be triggered to controllably release these particles (Shchukin *et al.* 2006, Sukhorukov *et al.* 2001). Finally, the motion of microcapsules on a surface can be regulated by nanoparticles that are adsorbed on the surface (Bhattacharya *et al*. 2009, Usta *et al.* 2008, Zhang *et al.* 2008).

With these microcapsules constituting the fundamental components of our system, we focus our attention on determining a minimal set of additives and conditions that will allow these objects to undergo collective haptotactic motion. To address this issue, we borrow basic concepts from cellular signaling in our design scheme. In particular, our simulations encompass two types of adaptive capsules, "signaling" and "target", which respectively release "agonists" and "antagonists" particles into the surrounding fluid. In cellular communication, dissolved agonists bind to the cell and promote the signaling process (production and release of the signal molecule), while antagonists that bind to the cell suppress these processes (Artyomov *et al*. 2007). In our model, the agonist and antagonist nanoparticles are designed to perform two functions: control the permeabilities of the capsules and alter the capsule-substrate interactions. Specifically, the permeabilities of both capsules (and hence, the particle release rates) depend on the local concentration of dissolved nanoparticles, so that the system exhibits a biomimetic feedback or self-regulating mechanism. Additionally, the released nanoparticles can adsorb onto the underlying substrate and thereby modify the wetting properties of the substrate.

The basic structural units in our simulations are spherical, fluid-filled elastic shells, which are immersed in a solution and localized on a substrate. Such fluid-filled elastic shells can serve as simple models for biological cells (e.g., leukocytes), as well as the polymeric microcapsules (Alexeev *et al.* 2005). In the simulations, the fluid dynamics of the encapsulated and the external solutions are captured via the lattice Boltzmann model (LBM), an efficient solver for the Navier-Stokes equation (Succi 2001). The capsule's elastic shell is simulated via the lattice spring model (LSM), which consists of a network of harmonic springs connecting regularly spaced masses (Ladd *et al*. 1997) by varying the spring constants for these bonds, we can alter the shell's mechanical compliance. Our integrated "LBM/LSM" approach (Alexeev *et al.* 2005, Alexeev *et al.* 2006) allows for a dynamic interaction between the elastic walls and the surrounding fluid as the moving walls exert a force on

the fluid and, in turn, the fluid reacts back on the walls. Below, we provide greater detail about our computational approach and then describe our findings on the three-dimensional behavior of pairs communicating, haptotactic microcapsules. We note that in our previous studies (Kolmakov et al. 2010), we demonstrated that multiple microcapsules can self-organize into various autonomously moving structures. In this paper, we specifically focus on analyzing the behavior of microcapsule pairs; understanding this elemental unit is crucial for designing more complicated, mobile assemblies.

2. Methodology

As noted above, we use our LBM/LSM approach to simulate adaptive, three-dimensional capsules that are localized on a surface and immersed in a host fluid. The capsule's elastic, solid shell is represented by a lattice spring model, which consists of a triangular network of harmonic springs that connect regularly spaced mass points, or nodes (Alexeev *et al.* 2007, Alexeev and Balazs 2007, Usta *et al.* 2007). The spring force $\mathbf{F}_s$ on node $\mathbf{r}_i$ is equal to

$$\mathbf{F}_s(\mathbf{r}_i) = -\sum_j k_j[(r_{ij} - r_{ij}^{eq})/r_{ij}]\mathbf{r}_{ij} \tag{1}$$

where the summation runs over all nearest- and next-nearest-neighbor nodes. The quantity $\mathbf{r}_{ij} = \mathbf{r}_i - \mathbf{r}_j$ is the radius vector between ith and jth nodes, r_{ij}^{eq} is the equilibrium length of the spring and k_j is the spring constant. To capture the dynamics of the solid shell, we numerically integrate Newton's equations of motion, $M(d^2\mathbf{r}_i/dt^2) = \mathbf{F}(\mathbf{r}_i)$, where M is the mass of a node. The total force $\mathbf{F}$ acting on a node consists of the following: the sum of the spring forces between the masses (representing the elastic response of the solid shell), the force exerted by the fluid on the shell at the fluid-solid boundary, and the adhesion forces at the solid substrate (see below).

The capsule's spherical shell is formed from two concentric layers of LSM nodes; each layer contains $N = 122$ nodes. These two layers are separated by a distance of $\Delta x_{LSM} = 1.5\Delta x$, where Δx_{LSM} is the lattice spacing between nearest nodes in the LSM and Δx is the spacing in the LBM (see below). The outer radius of the shell was taken to be R=5Δx. For small deformations and $k_1/2 = k_{\sqrt{2}} \equiv k$, the LSM system obeys linear elasticity theory and results in a Young's modulus of $E = 5k_j/2\Delta x_{LSM}$. Here k_1 and $k_{\sqrt{2}}$ are the spring constants in the orthogonal and the diagonal directions, respectively (Buxton *et al*. 2001, Ladd *et al*. 1997).

The LBM can be viewed as an efficient solver for the Navier-Stokes equation (Succi 2001). Specifically, this lattice-based model consists of two processes: the propagation of fluid "particles" to neighboring lattice sites, and the subsequent collisions between particles when they reach a site. Here, the fluid particles are representative of mesoscopic portions of the fluid, and are described by a particle distribution function $f_i(\mathbf{r},t)$, which characterizes the mass density of fluid particles at a lattice node $\mathbf{r}$ and time t propagating in the direction i with a constant velocity $\mathbf{c}_i$. (The velocities $\mathbf{c}_i$ in ith direction are chosen so that fluid particles propagate from one lattice site to the next in exactly one time step Δt). The time evolution of these distribution functions is governed by a discretized Boltzmann equation (Succi 2001). In three-dimensional systems, the simulations involve a set of 19 particle velocity distribution functions at each node. The hydrodynamic quantities of interest are moments of the distribution function, i.e., the mass density $\rho = \sum_i f_i$, the momentum density $\mathbf{j} = \rho\mathbf{u} = \sum_i \mathbf{c}_i f_i$, with $\mathbf{u}$ being the local fluid velocity, and the momentum flux $\Pi = \sum_i \mathbf{c}_i \mathbf{c}_i f_i$.

In our LBM/LSM simulations, the fluid and solid phases interact through appropriate boundary

conditions (Alexeev *et al.* 2005, 2006, Buxton *et al.* 2005). In particular, lattice spring nodes that are situated at the solid-fluid interface impose their velocities on the surrounding fluids; the velocities are transmitted through a linked bounce-back rule (Lallemand and Luo 2000) to those LBM distribution functions that intersect the moving solid boundary. In turn, LS nodes at the solid-fluid interface experience forces due to the fluid pressure and viscous stresses at that boundary. We calculate the latter force based on the momentum exchange between the LBM particle and solid boundary, and then distribute this quantity as a load to the neighboring LS nodes.

The signaling capsule releases agonist nanoparticles and the target acts as source for antagonist nanoparticles. Each capsule in the simulation initially encases $N_p = 10^4$ nanoparticles. These nanoparticles can diffuse from the interior of the capsules into the surrounding solution and adsorb onto the underlying substrate. To capture the fact that a capsule having a diameter of roughly 10 microns can enclose a very high number of nanoparticles, we assume that the nanoparticle concentration is not depleted during the time scale of our simulations. At each time step Δt, we add $\Delta N_p = 500 \times P$ nanoparticles to the interior of the capsules (Verberg *et al*. 2006), where P is taken equal to P^s for the signaling capsules and P^t for the target capsules. (We do not add nanoparticles into dormant capsules, i.e., when $P = 0$). Given that the diameter of a nanoparticle ≈10 nm, we estimate that each microcapsule can initially encapsulate up to $\approx 10^9$ nanoparticles. Taking into account that the typical simulation time is $\sim 2\times 10^4$ numerical time units, we infer that not more than ~1% of the maximum number of encapsulated nanoparticles are released in the course of simulation.

To capture the diffusion of the agonists and antagonists within the encapsulated and host fluid, we use a Brownian dynamics model for the particles (Verberg *et al.* 2005, 2006, 2007). The nanoparticles trajectories obey a stochastic differential equation

$$d\mathbf{r}(t) = \mathbf{u}(\mathbf{r}, t)dt + \sqrt{2D_0}d\mathbf{W}(t) \tag{2}$$

where the first term describes the advection due to the local fluid velocity $\mathbf{u}(\mathbf{r},t)$ and the second term describes the particle's Brownian motion, with D_0 being the particle's diffusion coefficient and $d\mathbf{W}(t)$ being the differential of a Weiner process with unit variance. We neglect backflow effects (i.e., the impact of the particles motion on the flow field); the latter assumption is valid for submicron sized particles at relatively low concentrations. We also neglect the interactions between the particles. We use a first order Euler scheme method to solve Eq. (4) (Verberg *et al.* 2006). Note that an ensemble average of the particle trajectories computed from Eq. (4) is equivalent to solving the convection-diffusion equation for the concentration of nanoparticles (Szymchak and Ladd 2003, Ottinger 1996, Verberg *et al.* 2006).

In our model, the agonists and antagonists are designed to perform two functions: alter the capsule-substrate interactions and control the permeabilities of the capsules. Specifically, the diffusing nanoparticles can bind to the surface and there upon, modify the capsule-surface interaction (Usta *et al.* 2008). To capture this aspect of the model, we start by modeling the capsule-surface interaction via a non-specific Morse potential, $\phi(r) = \varepsilon_s\left(1 - \exp\left[-\frac{(r - r_0)}{\kappa}\right]\right)^2$, where ε_s and κ characterize the respective strength and range of the interaction potential. The variable r represents the distance between lattice nodes on the capsule's outer surface and the substrate, which is also composed of lattice nodes, and r_0 is the distance where this force equals zero. In all our simulations, we set $\kappa = 1$ and $r_0 = 1$. In our model, diffusing agonists that bind to the surface increase the strength of the capsule-surface interaction and bound antagonists decrease this quantity. Thus, ε_s is written as $\varepsilon_s = \varepsilon(1-\theta+\theta')$, where ε is the adhesive strength of the bare surface, θ is fractional coverage of the surface by the

antagonists and θ' is the corresponding value for the agonists.

In our previous studies, we demonstrated that the fluid-driven motion of a deformable microcapsule along a surface is controlled by the elastic properties of the capsule's shell and substrate, as well as the capsule-surface adhesion (see Alexeev *et al*. 2005, 2006 for more details). In the simulations presented here, we focus on the motion of rigid capsules. Given that V is the capsule velocity, and μ is the fluid viscosity, we specifically consider cases where both the dimensionless capillary number, $Ca = V\mu / E\Delta x_{LSM}$, and the capsule-surface interaction strength, $\Phi = \varepsilon N / E\Delta x_{LSM}\kappa^2$, are small and, hence, the capsules' shapes are close to spherical (Verberg *et al*. 2006). In what follows, we set the interaction strength $\Phi = 10^{-2}$ and checked that in simulations $Ca < 10^{-4}$. In future studies, we will consider the effect that mechanical deformation of the capsules' shells has on the behavior of the system.

The permeabilities of the capsules shells (and, hence, the particle release rates) depend on the local concentration of dissolved particles. To capture the microcapsules' response to the variations in the concentration of agonist, C^t, and antagonist particles, C^s, we model the dependence of the permeability of the capsules' shells in the form of smoothed step functions

$$P^s = \frac{1}{2}P^s_{\max}\left(1 - \tanh\left(\frac{C^s - C_{thresh}}{\Delta C}\right)\right), \quad P^t = \frac{1}{2}P^t_{\max}\left(1 + \tanh\left(\frac{C^t - C_{thresh}}{\Delta C}\right)\right) \tag{3}$$

Here $P^s_{\max}$ and $P^t_{\max}$ are the maximum permeabilities of the signalling and target capsules' shells, respectively. In the present simulations, the sharpness of the transition from a "dormant" state with zero permeability of the capsule's shells to an "active" state with maximum permeability was taken equal to $\Delta C = 0.1 \times C_{thresh}$. We also set the threshold concentration for this transition, C_{thresh}, equal for the signaling and target capsules.

Finally, we note that recent experiments (Fiddes *et al.* 2009) have verified our two-dimensional (2D) LBM/LSM simulations (Zhu *et al*. 2007, 2007a) on the flow-driven movement of compliant capsules through narrow constrictions. Additionally, our 2D simulations for the steady-state motion of rigid particles inside a straight channel show quantitative agreement with corresponding finite element calculations (Zhu *et al.* 2007a). We validated our 3D LBM/LSM model by determining the drag force on a periodic array of spheres, as well as simulating the breathing mode oscillations of a single capsule. In both cases, the simulations showed quantitative agreement with analytical theory (Alexeev *et al*. 2005).

3. Results and discussion

To illustrate the adaptive, self-regulating behavior within our two-capsule system, we first just focus on stationary signaling and target microcapsules, neglecting the capsule-surface interactions. The plot in Fig. 1 indicates how the permeabilities of the capsules' shells, P^s and P^t, depend on local concentration of agonist and antagonist in the surrounding solution. The permeability of signal capsule's shell is initially $P^s_{\max}$. The agonists point particles are released from a source within the signaling capsule. The target capsule (Fig. 1(b)) also has a permeable shell and this permeability is initially characterized by $P^t_{\max}$. When the concentration of diffusing agonists around the target capsule is higher than the threshold value C^t_{thresh}, the target releases antagonist, which also diffuse in the solution. Eventually, the concentration of the antagonists around the signaling capsule exceeds a critical threshold C^s_{thresh}; subsequently, the permeability of the signaling capsule decreases as shown in

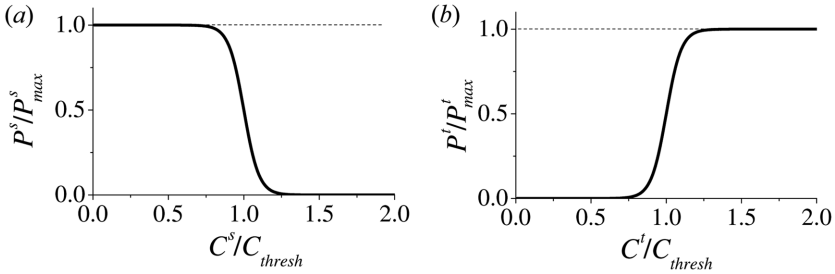

Fig. 1 Dependence of permeabilities P^s and P^t on the respective concentrations of antagonists (C^s) and agonists (C^t) in the solution

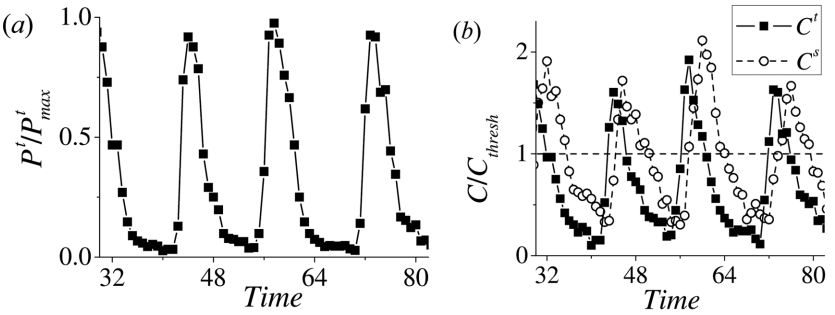

Fig. 2 (a) Oscillations in the permeability of the stationary target capsule. Here $P^t_{\max}/P^s_{\max} = 1$ and $C_{thresh} = 7.7$ (b) Oscillations in the concentration of agonist nanoparticles in solution at the target capsule, C^t (filled squares), and of antagonists at the signaling capsule, C^s (open circles). Time is normalized to the characteristic diffusion time R^2/D_f, where R is the capsule radius and D_f is the diffusion coefficient of the nanoparticles in solution

Fig. 1(a). Hence, the signaling capsule releases less agonist. (Here, we set $C^t_{thresh} = C^s_{thresh} \equiv C_{thresh}$).

At this stage, the small fraction of diffusing agonist causes the target capsule to release fewer antagonists since P^t also depends on the local concentration of agonists (see Fig. 1(b)). This small concentration of antagonist eventually diffuses away and has little effect on the signaling capsule. In this manner, the system is essentially reset, so that the signaling capsule again emits a high concentration of agonists and the entire cycle repeats.

Due to the positive and negative feedback mechanisms described above, the system exhibits self-sustained oscillations, which are evidenced in the plots in Fig. 2. In particular, Fig. 2(a) shows the value of P^t as a function of time, clearly revealing the periodic variations that occur due to the biomimetic self-regulating behavior. The plot for P^s as a function of time displays a similar temporal pattern. The rhythmic changes in P^t and P^s lead to oscillations in the concentration of agonist and antagonist in the solution, as can be seen in Fig. 2(b), where the squares represent the concentration of agonist and the circles represent the concentration of antagonist.

Having characterized the "information" exchange that occurs between the capsules via the nanoparticles in the solution, we now analyze how nanoparticles that adsorb on the surface affect the inter-capsule communication. In Fig. 3, we plot the changes in the adhesion strength along a line that is drawn through the two capsules' centers; specifically, we plot $\Delta\theta = \theta - \theta'$ along x'. Recall that θ' is the fractional surface coverage provided by the agonists and θ is the corresponding value for the antagonists; thus, a negative $\Delta\theta$ corresponds to a more adhesive region. At the onset, the

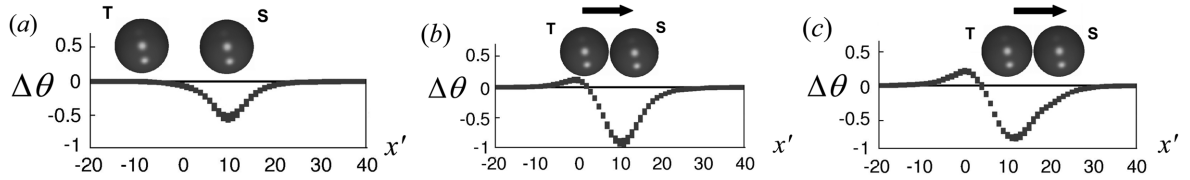

Fig. 3 Changes in the adhesion strength as measured by $\Delta\theta = \theta - \theta'$, and the subsequent capsule motion. Negative $\Delta\theta$ corresponds to a more adhesive region. S marks the signaling capsule and T marks the target capsule; x' is the spatial coordinate that is drawn through the capsules' centers

signaling capsule emits agonists; the bound agonists leave a "sticky" symmetric ring around this capsule; in Fig. 3(a), this appears as a uniform well under the signaling capsule.

As more agonists adsorb onto the surface, the well in Fig. 3(a) becomes deeper and soon creates an adhesion gradient near the target. If the adhesion profile is sufficiently asymmetric, a capsule is driven by enthalpic forces to spontaneously move from a less adhesive to a more adhesive area (Usta *et al.* 2008). And hence, due to the gradient, the target moves closer to the signaling capsule (i.e., in the direction of greater adhesion). Due to its greater proximity to the signaling capsule, the target now becomes activated and releases antagonists, which make the surface less "sticky" (indicated by the bump in Fig. 3(b)). Consequently, the adhesion profile in the region between the target and the signaling capsules is no longer symmetric and now both capsules move away from the less adhesive region towards the sticker area. The movement of the agonist-emitting signaling capsule further shifts the adhesion profile and again the pair moves towards the more attractive region around the signaling unit (see Fig. 3(c)). At this point, the entire process repeats, so that both capsules continue to move as a pair along the plane.

The plot in Fig. 4(a) is a three-dimensional representation of the scenario in Fig. 3(c). Here, the regions of weaker capsule-surface attraction are indicated as light-colored "hills" and the areas of stronger attraction are marked as darker valleys. As can be seen, the pair of capsules move from the "hills" toward the area that is made more attractive by the relatively high fraction of bound agonists ($\theta' > \theta$).

It is noteworthy that the deposition of both the agonists and antagonists are necessary for the directed movement of the pair in three dimensions. In contrast, for capsules moving along a line (i.e., in 2D simulations), the self-propelled motion can be achieved with antagonists alone (Usta *et al.* 2008).

To generate the images in Figs. 3 and 4, we set $P^t_{\max}/P^s_{\max} = 0.25$ and $C_{thresh} = 2.3$. The simulations revealed that both these parameters control the dynamic behavior of the pair, and the phase map is

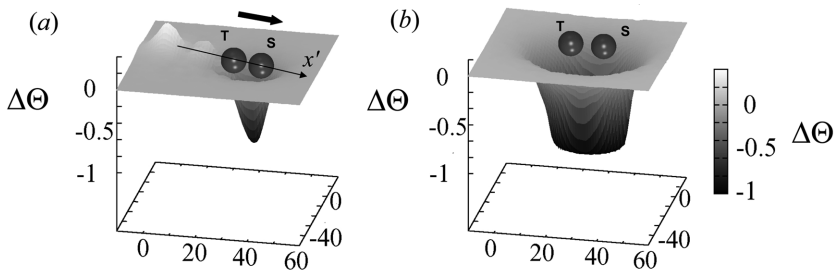

Fig. 4 Adhesion strength $\Delta\theta$ on the surface around: (a) a moving pair and (b) a pair that stops due to the saturation of the surface by agonist particles. Here $P^t_{\max}/P^s_{\max} = 0.25$; in (a), $C_{thresh} = 2.3$ and in (b), 13.1

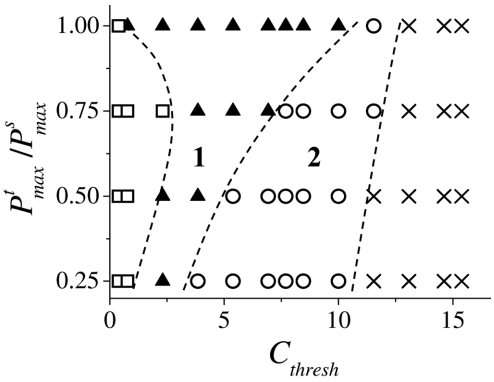

Fig. 5 Phase map depicting different regimes for the motion of the pair of microcapsules. Open squares: the target capsule orbits around the signaling capsule; filled triangles: directed, linear motion of the pair (Regime 1); open circles: the pair initially moves in concentric circles (Regime 2); crosses: the pair eventually comes to a halt (in the time scale of the simulation)

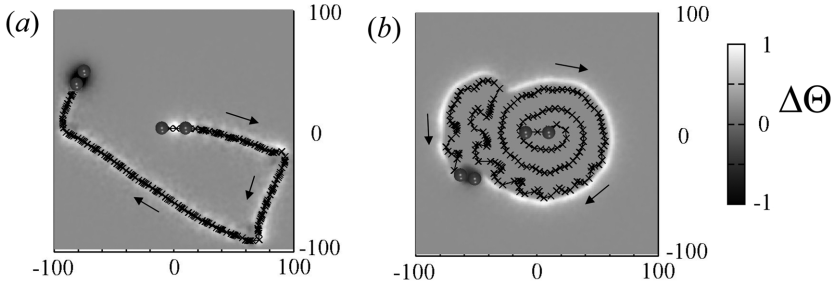

Fig. 6 Two modes of pair motion: (a) directed motion ($C_{thresh} = 2.3$) and (b) motion in concentric circles that then changes to a zigzag motion ($C_{thresh} = 8.5$); $P^t_{\max}/P^s_{\max} = 0.25$ in both cases. For the latter case, a significant concentration of antagonists is released into the system before the responsive signaling capsule releases the counteracting agonists. As a result, the surface becomes covered with the "less sticky" nanoparticles. This is evident by the light regions in Fig. 6(b)

shown in Fig. 5. Within this parameter space, we observed four distinct regimes. In the region indicated by the triangles (Regime 1), the pair moves in a directed, linear fashion; an example of this motion is shown in Fig. 6(a). (The capsules are initially placed near the point (0,0).) To better understand this system's dynamics, it is useful to examine the velocity for the center of mass of the two capsules. The plot in Fig. 7 shows that for $C_{thresh} = 2.3$ this velocity oscillates in time; in effect, the pair repeatedly stops and starts as they undergo their directed movement. The peaks in the latter plot correspond to the relatively rapid motion of the target capsule from a less adhesive to a more adhesive region in the vicinity of the signaling capsule (as in Figs. 3(b) and (c)).

Regime 1 occurs predominately at relatively low values of the threshold concentration C_{thresh}. As in the case of the two stationary capsules, which yielded oscillations in the permeabilities (see Fig. 2), the mobile capsules also exhibit oscillations in P^t and P^s, as shown in Fig. 8(a) for the case of $P^t_{\max}/P^s_{\max}=0.25$. (Once the target begins to release antagonists, the emissions from the signaling capsule are suppressed; it is for this reason that both the permeabilities oscillate in the range of roughly 0 to 7). Thus, within this regime, the self-regulating mechanism and corresponding oscillations in the concentrations of the dissolved agonist and antagonist (see Fig. 9(a)) play a critical role in directing the pair's movement.

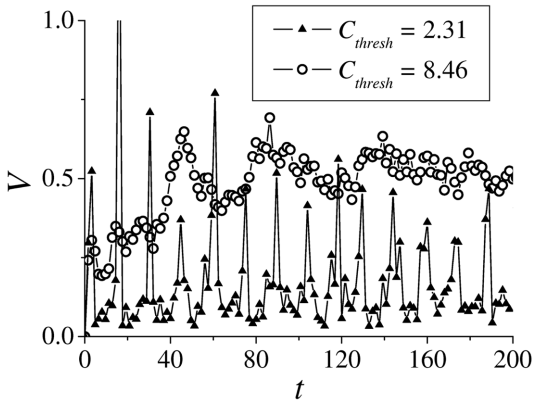

Fig. 7 Dependence on time of the center-of-mass velocity of the pair plotted for the cases shown in Fig. 6(a) $C_{thresh} = 2.3$ and (b) $C_{thresh} = 8.5$; $P^t_{\max}/P^s_{\max} = 0.25$. Time is normalized by the diffusion time R^2/D_f, and velocity is normalized by D_f/R

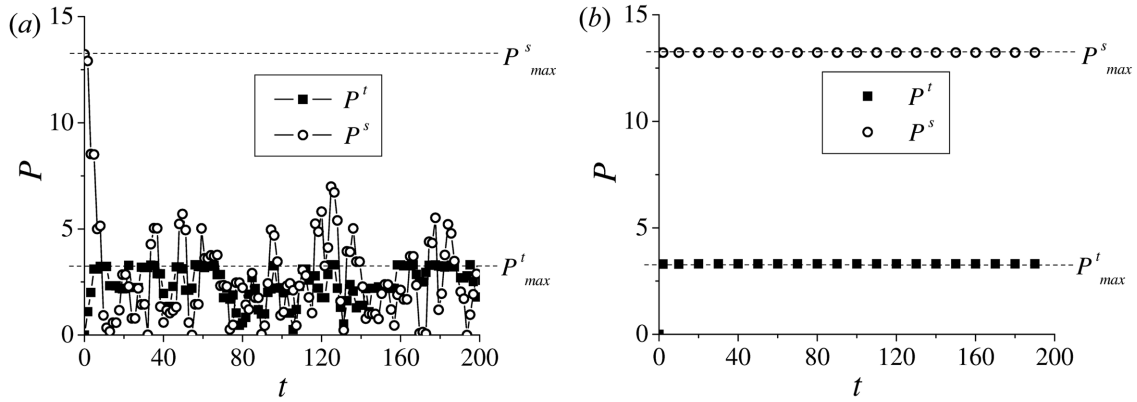

Fig. 8 Time dependence of the permeabilities of the signaling and target capsules plotted for directed (a) and concentric (b) modes, shown respectively in Figs. 6(a) and (b). (a) $C_{thresh} = 2.3$, (b) $C_{thresh} = 8.5$. $P^t_{\max}/P^s_{\max} = 0.25$ in both cases

A second distinct regime (Regime 2) occurs at higher C_{thresh} and is marked by the open circles on the phase map in Fig. 5. The motion of this pair shows less dramatic oscillations (Fig. 7) and the pair moves in a more continuous manner. In this regime, however, the linear motion of the capsules is unstable. The pair initially moves in concentric circles (see Fig. 6(b)) and at later times, undergoes a "zigzag" motion.

In Regime 2, which occurs at higher C_{thresh} and primarily at $P^t_{\max}/P^s_{\max} < 1$, we in fact see that the permeabilities of the capsules do not oscillate in time (Fig. 8(b)). Here, the signaling capsule must release a high concentration of agonists before the target is "switched on". Once the target is turned on, however, it does not release enough antagonist to suppress the signaling capsule (because $P^t_{\max}/P^s_{\max}$). Consequently, both the target and signaling are constantly releasing particles, with a relatively high concentration of agonists around the target and a relatively lower concentration of antagonists around the signaling capsule. Fig. 9(b) indeed shows that the concentrations of the different particles in the solution are relatively constant (the squares represent the concentration of agonist and the circles represent the concentration of antagonist.) In essence, the self-regulating

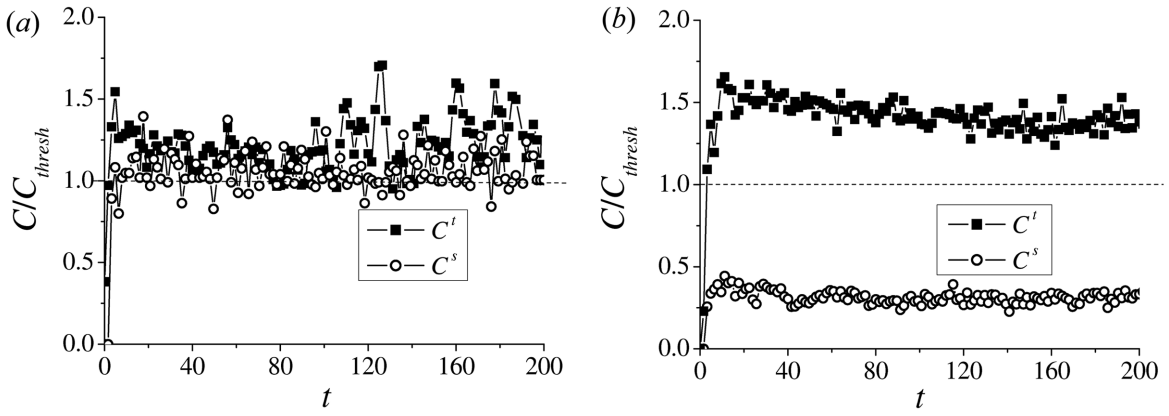

Fig. 9 Time dependence of the concentration of agonists, C^t, and antagonists, C^s, for: (a) directed motion and (b) motion in concentric circles. The dependences are plotted for the cases shown in Figs. 6(a) and (b), respectively

mechanism is not operative within this regime. This lack of self-regulation and the resulting constant flux of particles give rise to the erratic motion seen in Fig. 6b.

Within Regime 2, as the ratio $P^t_{\max}/P^s_{\max}$ becomes smaller, the target capsule releases less antagonists and the state where both capsules are "active" can be reached more readily; as a result, this regime becomes broader at lower $P^t_{\max}/P^s_{\max}$. For example, at $P^t_{\max}/P^s_{\max} = 0.25$, the pair exhibits mostly this mode of motion.

If C_{thresh} is above that for Regime 2, the local concentration of agonist nanoparticles is not sufficient to trigger the target capsule to release antagonists, and the pair stops as the surface becomes saturated with the sticky agonists. This situation is marked by the X's in the phase map and is depicted in Fig. 4(b), where a pair of stationary capsules is struck in a flat-bottomed, deep well.

In the opposite limit of $C_{thresh} << 1$, even small concentrations of the antagonist nanoparticles cause a dramatic decrease in the permeability of the signaling capsule's shell; hence, the release rate of the agonist nanoparticles is small. The concentration of agonist nanoparticles on the surface is not sufficiently high to cause the linear motion. As a result, the motion of the pair becomes localized in space. In this mode, the target orbits around a predominately stationary signaling capsule. (It is worth noting that the motion of the target capsule is mostly unidirectional in this case). This regime is marked by the squares in Fig. 5. Due to fluctuations in the concentration of the dissolved nanoparticles, the target can temporarily leave this orbit and move away from the signaling capsule. At later times, however, the target returns to the signaling capsule (because the signaling capsule resumes releasing "sticky" agonists in the absence of the target), and then, it continues the orbiting motion. At $P^t_{\max}/P^s_{\max} = 0.25$, this motion persists for long times because of the relatively low release rate of the antagonists; hence, it takes longer for the surface to reach saturation. At $P^t_{\max}/P^s_{\max} \geq 0.5$, however, the target capsule only makes a few turns and then stops due to faster saturation of the surface by antagonist nanoparticles.

From the above discussion, it appears that the step-like motion that characterizes the motion in Regime 1 is necessary for achieving the unidirectional movement. In other words, the positive and negative feedback that constitutes the self-regulating mechanism is vital for the generating this behavior. We note that hydrodynamic interactions also play a critical role within the system. In our computational approach, we can neglect hydrodynamics by removing the LBM component of the

simulations. In the absence of hydrodynamic interactions, the cases that previously exhibited concerted, linear motion could no longer sustain this behavior; instead, the particles were seen to just scatter. Hydrodynamic interactions play an important role because the capsules are moving through a viscous fluid, which mediates their motion. Specifically, the initial movement of the signaling capsule in the solution generates a net force (Usta *et al.* 2008) on the target that drives it to follow the signaling unit.

4. Conclusions

In conclusion, we incorporated a set of chemical reactions into a system of micro-carriers and thereby devised synthetic microscopic objects that modify their local environment, sense these modifications and effectively cooperate to move in response to these changes. These activities occur in the absence of an externally applied stimulus. Rather, the microcapsules carry with them necessary components for their self-propelled motion, which in turn emerges from basic physical and chemical phenomena. The multi-scale aspect of the simulations, which encompass not only the microcapsules, but also the diffusing nanoparticles and the surrounding fluid, allowed us to determine that the feedback mechanisms and hydrodynamic interactions are both necessary to achieve the unidirectional motion of a pair of capsules.

We note that there has been considerable interest recently in designing self-propelled, biomimetic particles (Ebben and Howse 2010, Hong *et al.* 2010, Sen *et al.* 2009) and cell-like droplets (Toyota *et al.* 2009). With respect to technological applications, the self-propelled microcapsules could pose a significant advantage: the robust, yet permeable shells in of the LbL microcapsules (Peyratout and Dahne 2004, Stadler *et al.* 2009) or of the "polymersomes" (Zhang *et al.* 2008) make these microscopic objects ideal carriers for transporting an encapsulated cargo to a specified location in a microfluidic device. In the scenario described here, the signaling capsule effectively transports the target and thus, the assembly could be harnessed to deliver this cargo in response to environmental changes in the system.

In these simulations, we use our recently developed hybrid, three-dimensional LSM/LBM approach, which allows us to capture the dynamic interactions between the capsule's elastic shell and surrounding fluids. We note that the LSM is equivalent to finite element approximations (Gusev 2004) of elastic solids (Rojek and Onate 2007, Shi and Tang 2008). The computational model presented here provides an ideal platform for determining additional parameters that can be used to regulate the motion of the self-propelled capsules. In particular, using this computational approach, we can modify the mechanical compliance of the capsules and the substrate. Furthermore, we can introduce multiple capsules, and vary the ratio of signaling to target capsules in the system. Thus, the method allows us to design a rich variety of structures and program complex self-organizing behaviors.

Finally, our model also provides a platform for integrating the spatial and temporal behavior of assemblies of biological cells with the reactions pathways associated with the signaling processes. As such, the approach can yield greater insight into the interrelationships among the signaling events, the movement of compliant cells and hydrodynamic interactions.

Acknowledgments

The authors gratefully acknowledge financial support from the DOE (for support of G.V.K) and ONR (for partial support of V.V.Y).

References

Alexeev, A., Verberg, R. and Balazs, A.C. (2005), "Modeling the motion of microcapsules on compliant polymeric surfaces", *Macromolecules*, **38**(24), 10244-10260.

Alexeev, A., Verberg, R. and Balazs, A.C. (2006), "Designing compliant substrates to regulate the motion of vesicles", *Phys. Rev. Lett*., **96**(14), 148103.

Alexeev, A. and Balazs, A.C. (2007), "Designing smart systems to selectively entrap and burst microcapsules", *Soft Matter*, **3**(12), 1500-1505.

Alexeev, A., Verberg, R. and Balazs, A.C. (2007), "Patterned surfaces segregate compliant microcapsules", *Langmuir*, **23**(3), 983-987.

Artyomov, M.N., Das, J., Kardar, M. and Chakraborty, A.K. (2007), "Purely stochastic binary decisions in cell signaling models without underlying deterministic bistabilities", *Proc. Natl. Acad. Sci. U.S.A*. **104**, 18958-18963.

Bellomo, E.G., Wyrsta, M.D., Pakstis, L., Pochan, D.J. and Deming, T.J. (2004), "Stimuli-responsive polypeptide vesicles by conformation-specific assembly", *Nature Mater.*, **3**, 244-248.

Bhattacharya, A., Usta, O.B., Yashin, V.V. and Balazs, A.C. (2009), "Self-sustained motion of a train of haptotactic microcapsules", *Langmuir,* **25**(17), 9644-9647.

Buxton, G.A., Care, C.M. and Cleaver, D.J. (2001), "A lattice spring model of heterogeneous material with plasticity", *Modelling Simul. Mater. Sci. Eng*., **9**(6), 485-497.

Buxton, G.A., Verberg, R., Jasnow, D. and Balazs, A.C. (2005), "Newtonian fluid meets an elastic solid: Coupling lattice Boltzmann and lattice-spring models", *Phys. Rev. E*, **71**(5), 056707.

Discher, B.M., Won, Y.Y., Ege, D.S., Lee, J.C.M., Bates, F.S., Discher, D.E. and Hammer, D.A. (1999), "Tough vesicles made from diblock copolymers", *Science*, **284**(5417), 1143-1146.

Ebbens, S.J. and Howse, J.R. (2010), "In pursuit of propulsion at the nanoscale", *Soft Matter*, **6**(4), 726-738.

Hammer, D.A., Robbins, G.P., Haun, J.B., Lin, J.J., Qi, W., Smith, L.A., Ghoroghchian, P.P., Therien, M.J. and Bates, F.S. (2008), "Leuko-polymersomes", *Faraday Discuss*., **139**, 129-141.

Fiddes, L.K., Chan, H.K.C., Wyss, K., Simmons, C.A., Kumacheva, E. and Wheeler, A.R., (2009), "Augmenting microgel flow via receptor-ligand binding in the constrained geometries of microchannels", *Lab Chip*, **9**, 286-290.

Hong, Y., Velegol, D., Chaturvedi, N. and Sen, A. (2010), "Biomimetic behavior of synthetic particles: from microscopic randomness to macroscopic control", *Phys. Chem. Chem. Phys*., **12**(7), 1423-1435.

Gusev, A.A., (2004), "Finite element mapping for spring network representations of the mechanics of solids", *Phys. Rev. Lett.,* **93**(3), 034302.

Jones, R.A.L. (2004), "Biomimetic polymers: tough and smart", *Nat. Mater.,* **3**, 209-210.

Kolmakov, G.V., Yashin, V.V., Levitan, S.P. and Balazs, A.C. (2010), "Designing communicating colonies of biomimetic microcapsules", *Proc. Natl. Acad. Sci.*, **107**(28), 12417-12422.

Ladd, A.J.C., Kinney, J.H. and Breunig, T.M. (1997), "Deformation and failure in cellular materials", *Phys. Rev. E,* **55**(3), 3271-3275.

Lallemand, P. and Luo, L.S. (2000), "Theory of the lattice Boltzmann method: Dispersion, dissipation, isotropy, Galilean invariance, and stability", *Phys. Rev. E*, **61**(6), 6546-6562.

Ma, Y., Dong, W.F., Hempenius, M.A., Mohwald, H. and Vancso, G.J. (2006), "Redox-controlled molecular permeability of composite-wall microcapsules", *Nat. Mater.,* 5, 724-729.

Nakata, S., Komoto, H., Hayashi, K. and Menzinger, M. (2000), "Mercury drop "attacks" an oxidant crystal", *J. Phys. Chem. B*, **104**(15), 3589-3593.

Ottinger, H.C. (1996), *Stochastic processes in polymeric fluids*, Springer, Berlin.

Peyratout, C.S. and Dahne, L. (2004), "Tailor-made polyelectrolyte microcapsules: From multilayers to smart containers", *Angew. Chem., Int. Edit.,* **43**(29), 3762-3783.

Rojek, J. and Onate, E., (2007), "Multiscale analysis using a coupled discrete/finite element model", *Interaction and Multiscale Mechanics*, **1**(1), 1-31.

Shi, G. and Tang, L., (2008), "Weak form of generalized governing equations in theory of elasticity", *Interaction and Multiscale Mechanics*, **1**(3), 329-337.

Solon, J., Streicher, P., Richter, R., Brochard-Wyart, F. and Bassereau, P. (2006), "Vesicles surfing on a lipid

bilayer: Self-induced haptotactic motion", *Proc. Natl. Acad. Sci. U.S.A*., **103**(33), 12382-12387.
Stadler, B., Price, A.D., Chandrawati, R., Hosta-Rigau, L., Zelikin, A.N. and Caruso, F. (2009), "Polymer hydrogel capsules: en route toward synthetic cellular systems", *Nanoscale,* **1**(1), 68-73.
Sen, A., Ibele, M. Hong, Y. and Velegol, D. (2009), "Chemo and phototactic nano/microbots", *Faraday Discuss.*, **143**, 15-27.
Shchukin, D.G., Zheludkevich, M., Yasakau, K., Lamaka, S., Ferreira, M.G.S. and Mohwald, H. (2006), "Layer-by-Layer assembled nanocontainers for self-healing corrosion protection", *Adv. Mater.,* **18(**13), 1672-1678.
Succi, S. (2001), *The lattice Boltzmann equation for fluid dynamics and beyond*, Clarendon Press, Oxford, UK.
Sukhorukov, G.B., Antipov, A.A., Voigt, A., Donath, E. and Mohwald, H. (2001), "pH-controlled macromolecule encapsulation in and release from polyelectrolyte multilayer nanocapsules", *Macromol. Rapid Comm.,* **22**(1), 44-46.
Sukhorukov, G., Fery, A. and Mohwald, H. (2005), "Intelligent micro- and nanocapsules", *Prog. Polym. Sci.*, **30**(8-9), 885-897.
Szymchak, P. and Ladd, A.J.C. (2003), "Boundary conditions for stochastic solutions of the convective-diffusion equations", *Phys. Rev. E,* **68**(3), 036704.
Tiourina, O.P., Radtchenko, I., Sukhorukov, G.B. and Mohwald, H. (2002), "Artificial cell based on lipid hollow polyelectrolyte microcapsules: Channel reconstruction and membrane potential measurement", *J. Membrane Biol.,* **190**(1), 9-16.
Toyota, T., Maru, N., Hanczyc, M.M., Ikegami, T. and Sugawara, T. (2009) "Self-propelled oil droplets consuming "fuel" surfactant", *J. Am. Chem. Soc.,* **131**(14), 5012-5013.
Usta, O.B., Alexeev, A. and Balazs, A.C. (2007), "Fork in the road: patterned surfaces direct microcapsules to make a decision", *Langmuir,* **23**(22), 10887-10890.
Usta, O.B., Alexeev, A., Zhu, G. and Balazs, A.C. (2008), "Modeling microcapsules that communicate through nanoparticles to undergo self-propelled motion", *ACS Nano*, **2**(3), 471-476.
Verberg, R, Yeomans, J.M., and Balazs, A.C. (2005), "Modeling the flow of fluid/particle mixtures in microchannels: Encapsulating nanoparticles within monodisperse droplets", *J. Chem Phys*., **123**, 224706.
Verberg, R., Alexeev, A. and Balazs, A.C. (2006), "Modeling the release of nanoparticles from mobile microcapsules", *J. Chem. Phys*., **125**, 224712.
Verberg, R., Dale, A.T., Kumar, P., Alexeev, A. and Balazs, A.C. (2007), "Healing substrates with mobile particle-filled microcapsules: Designing a 'repair and go' system", *J. R. Soc. Interface*, **4**(13), 349-357.
Weibel, D.B., Garstecki, P., Ryan, D., DiLuzio, W.R., Mayer, M., Seto, J.E. and Whitesides, G.M., (2005), "Microoxen: Microorganisms to move microscale loads", *Proc. Natl. Acad. Sci.*, **102**(34), 11963-11967.
Zhang, J., Srivastava, S., Duffadar, R., Davis, J.M., Rotello, V.M. and Santore, M.M. (2008), "Manipulating microparticles with single surface-immobilized nanoparticles", *Langmuir*, **24**(13), 6404-6408.
Zhu, G., Alexeev, A. and Balazs, A.C. (2007), "Designing constricted microchannels to selectively entrap soft particles", *Macromol.,* **40**(14), 5176-5181.
Zhu, G., Alexeev, A., Kumacheva, E. and Balazs, A.C. (2007a), "Modeling the interactions between compliant microcapsules and pillars in microchannels", *J. Chem. Phys.,* **127**, 034703.